

Influence of the symmetry energy and σ -cut potential on the properties of pure nucleonic and hyperon-rich neutron star matter

Prashant Thakur¹, B. K. Sharma², A. Ashika², S. Srivishnu² and T. K. Jha¹

¹*Department of Physics, BITS-Pilani, K. K. Birla Goa Campus, Goa 403726, India*

²*Department of Sciences, Amrita School of Physical Sciences, Amrita Vishwa Vidyapeetham, Coimbatore 641112, India*



(Received 6 November 2023; accepted 22 January 2024; published 21 February 2024)

We explore the influence of symmetry energy and the σ -cut potential on the properties of pure nucleonic and hyperon-rich neutron stars employing the relativistic mean-field (RMF) model with the S271 parameter set. The effects of symmetry energy are modulated by the Λ_ν coupling, while the σ -cut potential is governed by the free parameter f_s . The coupling constants between hyperons and mesons are ascertained based on the most recent hyperon-nucleon potentials derived from existing experimental data. Our analysis suggests that Λ_ν has more effect compared to f_s on the composition and global properties of neutron stars. Our results are consistent with various observational data, particularly with the GW170817 data.

DOI: [10.1103/PhysRevC.109.025805](https://doi.org/10.1103/PhysRevC.109.025805)

I. INTRODUCTION

Neutron stars are the collapsed cores of massive stars that underwent a supernova explosion and are made of matter that is squeezed to densities several times that of nuclear saturation density (n_0) [1,2]. At such high densities, neutron stars may not be composed of pure nucleonic matter, i.e., $npe\mu$ matter only. Recent discoveries of massive neutron stars suggest that there is a possibility that hyperons, heavier nonstrange bosons, kaons, boson condensate, and even deconfined quarks can occur inside the dense core of these stars. Therefore, neutron stars are ideal astrophysical objects to study nuclear matter under extreme conditions. The most important aspect of such studies is to construct the equation of state (EoS), which should be consistent with the experimental as well as observational data [3].

The experimental data from the finite nuclei studies provides crucial information about uniform symmetric nuclear matter in bulk around and slightly above the nuclear saturation density n_0 . For the high-density regime, i.e., above n_0 , such information is provided by the astrophysical observational data of neutron stars. For example, recent observations of massive pulsars such as PSR J1614-2230 [4,5], PSR J0348+0432 [3], and PSR J0740+6620 [6] point to the mass of such compact stars to be about twice the mass of the sun ($M \geq 2M_\odot$). Also, mass-radius measurements from PSR J0030+0451 [7-9] and from NICER (PSR J0740+6620) [10,11] suggest repulsive behavior of dense matter at high densities. The analysis of recent observational data from NICER as well as from the GW170817 event [12] further constrains the EoS and bulk properties of neutron stars, such as those on the tidal deformability ($\Lambda_{1.4}$) and radius ($R_{1.4}$) for a $1.4M_\odot$.

It is clearly evident that one has to construct a stiffer EoS at high-density regime to achieve high-mass configuration, which will then be consistent with recent observations of neutron stars. Several mechanisms, such as repulsive components

of hyperon-hyperon interaction [13,14], three-body hyperon-nucleon interaction [15,16], and quark phase [4], have been developed to make the EoS stiffer at high density. However, these mechanisms also affect the properties of nuclear matter around n_0 . To rectify this drawback, Maslov *et al.* proposed a σ -cut scheme [17], in which they introduce a σ -potential term, i.e., $U_{\text{cut}}(\sigma)$ in the relativistic mean field (RMF) Lagrangian, which reduces the contribution of the σ field and consequently makes the EoS stiffer at high density without affecting the nuclear matter properties at saturation density. Various research groups [18-21] have applied the σ -cut scheme to study the effect of the σ potential on normal and exotic forms of nuclear matter at low- and high-density regimes. Another important quantity that provides crucial information about neutron-rich matter at high density is nuclear symmetry energy (E_{sym}) and its density dependence [2,22]. The E_{sym} and its density dependence have a substantial effect on the pressure of neutron star matter and consequently affect their properties, especially the radius of neutron stars [23,24]. Despite being one of the important quantities of the EoS, nuclear symmetry energy and its high-density behavior are not well understood. However, many studies have been done to constrain the value of E_{sym} and its high-density behavior based on the data from terrestrial experiments as well as from astrophysical observations [25-27]. Recently, the improved value of the neutron skin thickness of ^{208}Pb around (0.283 ± 0.071) fm was reported in the Lead Radius EXperiment-II (PREX-2) [28]. The values of E_{sym} and its slope L with this neutron skin thickness are (38.1 ± 4.7) MeV and (106 ± 37) at n_0 , respectively [29]. The updated values of E_{sym} and L are larger compared to the previously reported values [1], which were obtained from the comparison of experimental data of finite nuclei and heavy-ion collisions with various microscopic model calculations.

The aim of this work is to investigate how the σ -cut potential and symmetry energy affect the properties of pure nucleonic and hyperon-rich neutron stars. In our analysis, pure

nucleonic and hyperon-rich matter stand for the matter that contains only nucleons and leptons, and the matter that contains hyperons along with nucleons and leptons, respectively. We include Λ_v coupling and σ -cut potential in our RMF model Lagrangian to incorporate their effect on the EoS and consequently on the properties of neutron stars with or without a hyperon core. For the present analysis, we choose the S271 parameter set [30] with $\Lambda_v = 0.00$ and 0.03 , and for the σ -cut potential, we take $f_s = 0.5$ and 0.6 , respectively.

The paper is organized as follows. A brief description of the theoretical framework for the present analysis is provided in Sec. II. We present and discuss our results in Sec. III. Finally, the conclusions and summary of the present work are given in Sec. IV.

II. THEORETICAL FRAMEWORK

In this section, we will briefly describe the essential features of the theoretical formalism that we apply in the present work.

A. Equation of state

We choose the well-established RMF model to describe the equation of state (EoS) for pure nucleonic and hyperon-rich neutron stars using the S271 parameter set. We consider all the octet of baryons (n , p , Λ , Σ , Ξ) and leptons (e , μ) as the composition of neutron star matter. In the RMF Lagrangian, we include $U_{\text{cut}}(\sigma)$ to make the EoS stiffer at high density, and the symmetry energy effect will be taken care of by Λ_v . The total Lagrangian density with $U_{\text{cut}}(\sigma)$ and Λ_v is given by:

$$\begin{aligned} \mathcal{L} = & \sum_B \bar{\Psi}_B (i\gamma^\mu D_\mu - M_B + g_{\sigma B}\sigma) \Psi_B + \frac{1}{2} \partial_\mu \sigma \partial^\mu \sigma \\ & - m_\sigma^2 \sigma^2 \left(\frac{1}{2} + \frac{\kappa_3}{3!} \frac{g_{\sigma N} \sigma}{M_N} + \frac{\kappa_4}{4!} \frac{g_{\sigma N}^2 \sigma^2}{M_N^2} \right) - \frac{1}{4} \Omega_{\mu\nu} \Omega^{\mu\nu} \\ & + \frac{1}{2} \left(1 + \eta_1 \frac{g_{\sigma N} \sigma}{M_N} + \frac{\eta_2}{2} \frac{g_{\sigma N}^2 \sigma^2}{M_N^2} \right) m_\omega^2 \omega_\mu \omega^\mu - \frac{1}{4} R_{\mu\nu}^a R^{a\mu\nu} \\ & + \frac{1}{2} \left(1 + \eta_\rho \frac{g_{\sigma N} \sigma}{M_N} \right) m_\rho^2 \rho_\mu^a \rho^{a\mu} + \frac{1}{4!} \zeta_0 g_{\omega N}^2 (\omega_\mu \omega^\mu)^2 \\ & + \Lambda_v g_{\omega N}^2 (\omega_\mu \omega^\mu) g_{\rho N}^2 (\rho_\mu \cdot \rho^\mu) - U_{\text{cut}}(\sigma). \end{aligned} \quad (1)$$

The symmetry energy $E_{\text{sym}}(\rho)$ of the above Lagrangian is given by:

$$E_{\text{sym}}(\rho) = \frac{k_F^2}{6E_F^*} + \frac{g_\rho^2}{12\pi^2} \frac{k_F^3}{m_\rho^{*2}}, \quad (2)$$

where $E_F^* = \sqrt{k_F^2 + M_N^{*2}}$, k_F and $M_N^* = M_N - g_{\sigma N} \sigma_0$ are the Fermi energy, Fermi momentum, and effective mass of the nucleon, respectively. The effective rho meson mass is $m_\rho^{*2} = m_\rho^2 + 2g_{\rho N}^2 (\Lambda_v g_\omega^2 \omega_0^2)$. The Λ_v coupling modifies the density dependence of the symmetry energy by m_ρ^{*2} without affecting the saturation properties. We take $\Lambda_v = 0.00$ and 0.03 for the present calculation. According to Eq. (2), we varied the value of Λ_v and adjusted $g_{\rho N}$ for each value of Λ_v such that the value of E_{sym} remains fixed at saturation density n_0 .

The $U_{\text{cut}}(\sigma)$ has a logarithmic form as in Ref. [17], which only influences the σ field at high density and is given by,

$$U_{\text{cut}}(\sigma) = \alpha \ln\{1 + \exp[\beta(g_{\sigma N} \sigma / M_N - f_s)]\}, \quad (3)$$

where $\alpha = m_\pi^4$ and $\beta = 120$ [17] to make the EoS stiffer at high density. The factor f_s is a free parameter and we take $f_s = 0.5$ and 0.6 for our calculation. The field equations for σ , ω , and ρ mesons obtained from Eq. (1) are given by:

$$\begin{aligned} m_\sigma^2 \left(\sigma_0 + \frac{g_{\sigma N} \kappa_3}{2M_N} \sigma_0^2 + \frac{g_{\sigma N}^2 \kappa_4}{6M_N^2} \sigma_0^3 \right) + U'_{\text{cut}}(\sigma) \\ - \frac{1}{2} m_\omega^2 \left(\eta_1 \frac{g_{\sigma N}}{M_N} + \eta_2 \frac{g_{\sigma N}^2}{M_N^2} \sigma_0 \right) \omega_0^2 \\ - \frac{1}{2} m_\rho^2 \eta_\rho \frac{g_{\sigma N}}{M_N} \rho_0^2 = \sum_B g_{\sigma B} M_B^{*2} n_{SB} \end{aligned} \quad (4)$$

$$\begin{aligned} m_\omega^2 \left(1 + \frac{\eta_1 g_{\sigma N}}{M_N} \sigma_0 + \frac{\eta_2 g_{\sigma N}^2}{2M_N^2} \sigma_0^2 \right) \omega_0 \\ + 2\Lambda_v g_{\omega N}^2 g_{\rho N}^2 \rho_0^2 \omega_0 + \frac{1}{6} \zeta_0 g_{\omega N}^2 \omega_0^3 = \sum_B g_{\omega B} n_B \end{aligned} \quad (5)$$

$$m_\rho^2 \left(1 + \frac{g_{\sigma N} \eta_\rho}{M_N} \sigma_0 \right) \rho_0 + 2\Lambda_v g_{\omega N}^2 g_{\rho N}^2 \omega_0^2 \rho_0 = \sum_B g_{\rho B} I_{3B} n_B, \quad (6)$$

where n_{SB} , n_B , and I_{3B} are the scalar baryon density, baryon number density, and the third component of the nucleon isospin operator, respectively. The derivative of $U_{\text{cut}}(\sigma)$ is given by:

$$U'_{\text{cut}}(\sigma) = \frac{\alpha \beta g_{\sigma N}}{M_N} \frac{1}{\{1 + \exp[\beta(g_{\sigma N} \sigma / M_N - f_s)]\}}. \quad (7)$$

The equation of state (EoS) for hyperon-rich matter should satisfy the conservation of total baryon number and charge neutrality condition, and is given by:

$$\sum_B Q_B n_B + \sum_L Q_L n_L = 0, \quad (8)$$

where n_B and n_L are the baryon and the lepton (e , μ) number densities with Q_B and Q_L as their respective electric charge.

The energy density \mathcal{E} and pressure P for charge-neutral, β -equilibrated neutron star matter with the lowest-lying octet of baryons are given by:

$$\begin{aligned} \mathcal{E} = & \sum_B \frac{2}{(2\pi)^3} \int_0^{k_B} d^3 k E_B^*(k) + \left(\sum_B g_{\omega B} n_B \right) \omega_0 \\ & + \left(\sum_B g_{\rho B} I_{3B} n_B \right) \rho_0 - \frac{1}{4!} \zeta_0 g_{\omega N}^2 \omega_0^4 + U_{\text{cut}}(\sigma) \\ & - \frac{1}{2} \left(1 + \frac{\eta_1 g_{\sigma N}}{M_N} \sigma_0 + \frac{\eta_2 g_{\sigma N}^2}{2M_N^2} \sigma_0^2 \right) m_\omega^2 \omega_0^2 \\ & + m_\sigma^2 \sigma_0^2 \left(\frac{1}{2} + \frac{\kappa_3 g_{\sigma N} \sigma_0}{3! M_N} + \frac{\kappa_4 g_{\sigma N}^2 \sigma_0^2}{4! M_N^2} \right) \\ & - \frac{1}{2} \left(1 + \eta_\rho \frac{g_{\sigma N} \sigma_0}{M_N} \right) m_\rho^2 \rho_0^2 - \Lambda_v g_{\omega N}^2 g_{\rho N}^2 \omega_0^2 \rho_0^2 + \sum_L \mathcal{E}_L \end{aligned} \quad (9)$$

$$\begin{aligned}
 P = & \sum_B \frac{2}{3(2\pi)^3} \int_0^{k_B} d^3k \frac{k^2}{E_B^*(k)} + \frac{1}{4!} \zeta_0 g_{\omega N}^2 \omega_0^4 - U_{\text{cut}}(\sigma) \\
 & + \frac{1}{2} \left(1 + \frac{\eta_1 g_{\sigma N}}{M_N} \sigma_0 + \frac{\eta_2 g_{\sigma N}^2}{2M_N^2} \sigma_0^2 \right) m_\omega^2 \omega_0^2 \\
 & - m_\sigma^2 \sigma_0^2 \left(\frac{1}{2} + \frac{\kappa_3 g_{\sigma N} \sigma_0}{3!M_N} + \frac{\kappa_4 g_{\sigma N}^2 \sigma_0^2}{4!M_N^2} \right) \\
 & + \frac{1}{2} \left(1 + \eta_\rho \frac{g_{\sigma N} \sigma_0}{M_N} \right) m_\rho^2 \rho_0^2 + \Lambda_\nu g_{\omega N}^2 g_{\rho N}^2 \omega_0^2 \rho_0^2 \\
 & + \sum_L P_L. \tag{10}
 \end{aligned}$$

Here the subscripts B , N , and L represent the low-lying octet of baryons, nucleons, and leptons, respectively. The \mathcal{E}_L and P_L are the energy density and pressure of the leptons. It is to be noted that the coupling constant of the ω^4 term, i.e., ζ_0 is equal to $g_{\omega N}^2 \zeta$ where ζ is defined as the coupling constant of the ω^4 term in Ref. [30]. As in Ref. [30], $\zeta = 0$ for the S271 parameter set, which implies that $\zeta_0 = 0$ in the present analysis.

B. Model parameters

We apply the SU(6) quark model to calculate the vector meson-hyperon coupling for S271.

$$g_{\omega\Lambda} = g_{\omega\Sigma} = g_{\omega\Xi} = \frac{2}{3} g_{\omega N} \tag{11}$$

$$g_{\rho\Lambda} = 0, g_{\rho\Sigma} = g_{\rho\Xi} = g_{\rho N}. \tag{12}$$

The σ meson coupling with hyperons is fixed by

$$U_H^N|_{n_0} = x_{\omega H} U_V|_{n_0} - x_{\sigma H} U_S|_{n_0}, \tag{13}$$

where $x_{\omega H} = g_{\omega H}/g_{\omega N}$, $x_{\sigma H} = g_{\sigma H}/g_{\sigma N}$ are the coupling constants for vector and scalar mesons, respectively. The $U_V|_{n_0}$ and $U_S|_{n_0}$ are values of ω and σ potentials at saturation density n_0 . Among hyperon-nucleon potential, U_Λ^N is well constrained compared to U_Σ^N and U_Ξ^N . The experimental data [31] suggest that U_Σ^N is repulsive, while U_Ξ^N is attractive. In this work, we take $U_\Lambda^N = -28$ MeV, $U_\Sigma^N = 30$ MeV, and $U_\Xi^N = -24$ MeV. The corresponding values of $x_{\sigma\Lambda}$, $x_{\sigma\Sigma}$, and $x_{\sigma\Xi}$ are 0.6134, 0.4070, and 0.3423, respectively, for S271.

C. Stellar equations and tidal deformability

The mass-radius relation for a neutron star is obtained by solving the Tolman, Oppenheimer, and Volkoff (TOV) equation [32,33], which is given by:

$$\frac{dP}{dr} = -\frac{G[\varepsilon + P][M + 4\pi r^3 P]}{r(r - 2GM)}, \tag{14}$$

$$\frac{dM}{dr} = 4\pi r^2 \varepsilon. \tag{15}$$

Here we adopt natural units, i.e., $c = 1$, G , $P(r)$ and $M(r)$ are the universal gravitational constant, pressure of a neutron star, and the enclosed gravitational mass inside a sphere of radius (r) , respectively. Equations (14) and (15) are solved to obtain

the structural properties of a static neutron star with charge neutral hyperonic matter [34,35].

The tidal deformability parameter λ is defined as [36–39]:

$$Q_{ij} = -\lambda \mathcal{E}_{ij}, \tag{16}$$

where Q_{ij} is the induced quadrupole moment of a star in a binary due to the static external tidal field \mathcal{E}_{ij} of the companion star. The parameter λ can be expressed in terms of the dimensionless quadrupole tidal Love number k_2 as:

$$\lambda = \frac{2}{3} k_2 R^5, \tag{17}$$

where R is the radius of the NS. The value of k_2 is typically in the range $\simeq 0.05$ – 0.15 [37,38,40] for NSs and depends on the stellar structure. This quantity can be calculated using the following expression [37]:

$$\begin{aligned}
 k_2 = & \frac{8C^5}{5} (1 - 2C)^2 [2 + 2C(y_R - 1) - y_R] \\
 & \times \{ 2C[6 - 3y_R + 3C(5y_R - 8)] \\
 & + 4C^3[13 - 11y_R + C(3y_R - 2) + 2C^2(1 + y_R)] \\
 & + 3(1 - 2C)^2 [2 - y_R + 2C(y_R - 1)] \log(1 - 2C) \}^{-1}, \tag{18}
 \end{aligned}$$

where $C (\equiv M/R)$ is the compactness parameter of the star with mass M . The quantity $y_R [\equiv y(R)]$ can be obtained by solving the following differential equation:

$$r \frac{dy(r)}{dr} + y(r)^2 + y(r)F(r) + r^2 Q(r) = 0, \tag{19}$$

with

$$F(r) = \frac{r - 4\pi r^3 [\varepsilon(r) - P(r)]}{r - 2M(r)}, \tag{20}$$

$$\begin{aligned}
 Q(r) = & \frac{4\pi r \left(5\varepsilon(r) + 9P(r) + \frac{\varepsilon(r)+P(r)}{\partial P(r)/\partial \varepsilon(r)} - \frac{6}{4\pi r^2} \right)}{r - 2M(r)} \\
 & - 4 \left[\frac{M(r) + 4\pi r^3 P(r)}{r^2 [1 - 2M(r)/r]} \right]^2. \tag{21}
 \end{aligned}$$

In the previous equations, $M(r)$ is the mass enclosed within the radius r , and $\varepsilon(r)$ and $P(r)$ are the energy density and pressure in terms of the radial coordinate r of a star, respectively. These quantities are calculated within the nuclear matter model chosen to describe the stellar EoS. For a given EoS, Eq. (19) can be integrated together with the Tolman-Oppenheimer-Volkoff equations with the boundary conditions $y(0) = 2$, $P(0) = P_c$, and $M(0) = 0$, where $y(0)$, P_c , and $M(0)$ are the dimensionless quantity, pressure, and mass at the center of the NS, respectively. One can then define the dimensionless tidal deformability as $\Lambda = \frac{2}{3} k_2 C^{-5}$.

III. RESULTS AND DISCUSSION

In this work, we construct the equation of state (EoS) for neutron stars composed of only nucleons and nucleons plus hyperons matter within the RMF model. We include the Λ_ν and σ -cut potential in the formalism to examine their effect on the properties of neutron stars. We choose the S271 parameter

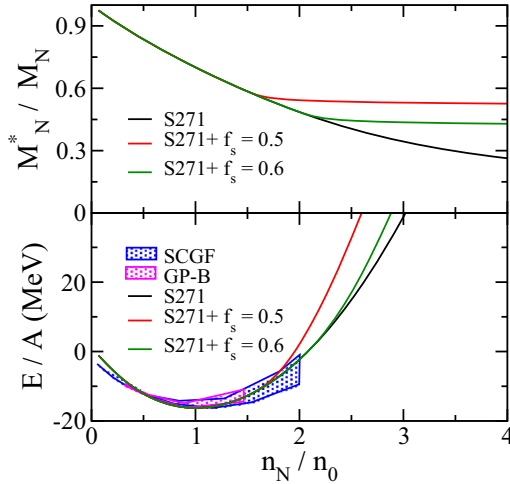


FIG. 1. The effective mass (in units of M_N) and total energy per nucleon as a function of nucleon number density n_N (in units of n_0) of symmetric nuclear matter are shown in the top and bottom panels. The blue shaded region in the bottom panel is the result from the *ab initio* nonperturbative self-consistent Green's function (SCGF) approach with chiral forces [42], and the magenta shaded region represents the 1σ uncertainty band derived from chiral effective theory [43], respectively.

set [30] for our present analysis because the nonlinear coupling of the ω meson is zero like NL3 [41], which makes the EoS stiffer at high density. In Ref. [18], Zhang *et al.* show that the parameter f_s is a free parameter in the σ -cut potential and its value of 0.5 and above is suitable for high-density nuclear matter. We choose S271 along with the σ -cut potential, i.e., $f_s = 0.5$ and 0.6 and compare our results with S271. We choose $\Lambda_v = 0.00$ and 0.03 to incorporate the high-density behavior of the symmetry energy in the present work. It is to be noted that Λ_v and the σ -cut potential have no contribution in the S271 parameter set [30]. So, the results for the S271 parameter set with $\Lambda_v = 0.00$ and without the σ -cut potential reproduce the original S271 parameter set.

Before we proceed with the results on the influence of the σ -cut potential and Λ_v on the properties of neutron stars, we present our results for symmetric nuclear matter in Fig. 1. Only the σ -cut potential affects the properties of symmetric nuclear matter because Λ_v , which is the cross coupling of the ω - ρ term, does not contribute here. The σ -cut potential affects nuclear matter properties by changing the σ -meson field contribution. The total energy per nucleon (E/A) and effective nucleon mass (M_N^*) of symmetric nuclear matter are the properties that depend on the σ -meson contribution. So, the σ -cut potential has a significant effect on these two properties. The effective nucleon mass, normalized to M_N , and the total energy per nucleon (E/A) as a function of nucleon number density (n_N) normalized to n_0 , are shown in the top and bottom panels of Fig. 1, respectively. For the S271 parameter set, the effective nucleon mass is monotonically decreasing with increasing n_N , like other interactions based on the RMF model. From the top panel of Fig. 1, we find that the σ -cut potential has no effect on the effective nucleon mass at the saturation density n_0 . We also find that the σ -cut potential influences the

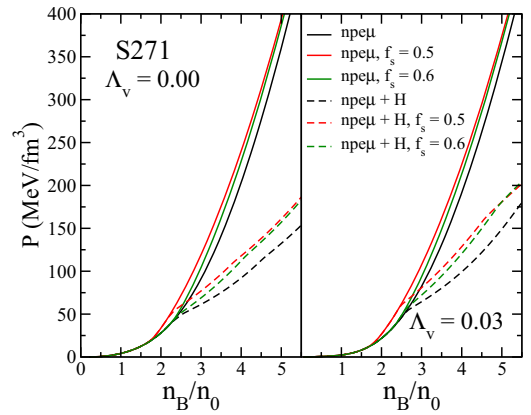


FIG. 2. The pressure as a function of baryon number density n_B (in units of n_0) for $\Lambda_v = 0.00$ (left panel) and $\Lambda_v = 0.03$ (right panel) with S271 and S271 with $f_s = 0.5$ and 0.6, respectively.

effective nucleon mass at lower densities, around $1.58n_0$ for $f_s = 0.5$ compared to $2.14n_0$ for $f_s = 0.6$, respectively. We found a similar influence of the σ -cut potential on the total energy per nucleon for $f_s = 0.5$ and 0.6.

From the bottom panel of Fig. 1, we see that the E/A increases with increasing n_N . We also display the results from *ab initio* nonperturbative self-consistent Green's function (SCGF) approach [42], as well as the 1σ uncertainty band (GP-B) derived from the chiral effective theory using a Bayesian approach based on Gaussian process [43], and compare them with our results for S271 and S271 with $f_s = 0.5$ and 0.6. We found that our results are quite consistent with them. We see that the σ -cut potential does not affect the total energy per nucleon at n_0 for the three EoS. The σ -cut potential affects the total energy per nucleon at the same density as the effective nucleon mass. Also, the σ -cut potential influences the E/A at low nucleon density for $f_s = 0.5$ as compared to $f_s = 0.6$. So, from Fig. 1, we can conclude that the σ -cut potential has no effect at n_0 , and its effect is more prominent at higher densities, which play a crucial role in determining the properties of neutron stars.

The equation of state (EoS), i.e., the variations in the pressure of a pure nucleonic and hyperon-rich neutron star as a function of the baryon number density n_B , normalized to n_0 is presented in the Fig. 2. The EoS of pure nucleonic and hyperon-rich neutron star for the S271 parameter set is shown as solid and dashed black lines in the left panel of Fig. 2. In the S271 parameter set, the pressure profile for pure nucleonic neutron stars is stiffer compared to hyperon-rich neutron stars at high densities. The equation of state (EoS) of pure nucleonic and hyperon-rich neutron stars for S271 with $f_s = 0.5$ and 0.6 is also shown in the left panel in Fig. 2. For pure nucleonic neutron stars, the pressure profile becomes stiffer at lower n_B values, particularly around $1.85n_0$ for $f_s = 0.5$, in contrast to $2.48n_0$ for $f_s = 0.6$. Like S271, as n_B increases from $2n_0$ to $5n_0$, the pressure profiles for both values of f_s converge. Similarly, the pressure of pure nucleonic neutron stars becomes stiffer at higher n_B compared to hyperon-rich neutron stars like the S271 parameter set. So, one can conclude that the overall trend of pressure profiles with n_B is

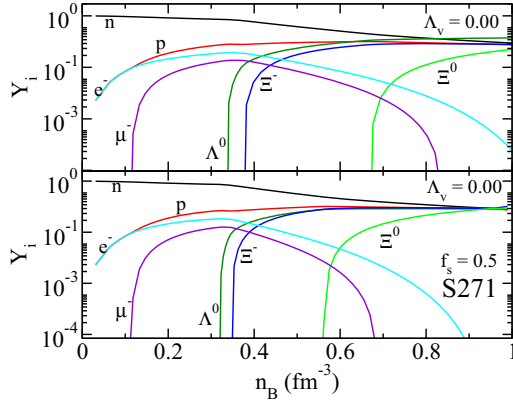


FIG. 3. The particle fractions Y_i of baryons and leptons as a function of baryon number density n_B in a neutron star with S271 (top panel) and S271 with $f_s = 0.5$ (bottom panel) for $\Lambda_v = 0.00$.

similar for S271 and S271 with $f_s = 0.5$ and 0.6 . In the right panel of Fig. 2, we present our results with $\Lambda_v = 0.03$ for S271 and S271 with $f_s = 0.5$ and 0.6 for pure nucleonic and hyperon-rich neutron stars, respectively. However, the overall trend of EoS with $\Lambda_v = 0.03$ for pure nucleonic and hyperon-rich neutron stars does not alter significantly compared to the left panel. However, from the analysis of both panels of Fig. 2, it is evident that Λ_v has a slight effect on the equation of state (EoS) of pure nucleonic and hyperon-rich neutron stars. Minor pressure variations are observed in hyperon-rich neutron stars at elevated n_B levels for different f_s values in both panels of Fig. 2. Hence, it is evident that f_s has a slightly more effect on the EoS compared to Λ_v .

The particle fractions Y_i of baryons and leptons are plotted against the number density n_B . The top panel of Fig. 3 belongs to S271 and the bottom panel corresponds to S271 with $f_s = 0.5$, respectively. The value $f_s = 0.5$ was selected for comparative analysis with the S271 parameter set due to its stiffer pressure profile about n_B . Also, a slight pressure difference is observed in neutron stars with a hyperon core between $f_s = 0.5$ and $f_s = 0.6$, which indicates a minor influence on the hyperon occurrence for these values of f_s . The onset of Λ^0 hyperons occurs at around $n_B = 0.34 \text{ fm}^{-3}$ and $n_B = 0.32 \text{ fm}^{-3}$ for the S271 parameter set and S271 with $f_s = 0.5$, respectively. Also, Ξ^- and Ξ^0 appears at $n_B = 0.38 \text{ fm}^{-3}$ and $n_B = 0.67 \text{ fm}^{-3}$ for the S271 parameter set, respectively. Similarly, Ξ^- and Ξ^0 occur at $n_B = 0.35 \text{ fm}^{-3}$ and $n_B = 0.56 \text{ fm}^{-3}$ for S271 with $f_s = 0.5$, respectively. From Fig. 3, it is evident that for S271 with $f_s = 0.5$, the onset of hyperons happens at a low value of n_B compared to the S271 parameter set, and this feature is more prominent for Ξ 's hyperons.

We extend our analysis of particle fractions Y_i in hyperon-rich neutron stars for $\Lambda_v = 0.03$, which is shown in Fig. 4. The particle fractions Y_i of baryons and leptons are plotted as a function of n_B and shown in the top and bottom panels of Fig. 4, which correspond to the S271 parameter set and S271 with $f_s = 0.5$ for $\Lambda_v = 0.03$, respectively. As from Fig. 3, we found that the hyperons appear relatively earlier (at a lower value of n_B) for S271 with $f_s = 0.5$ compared to S271. The

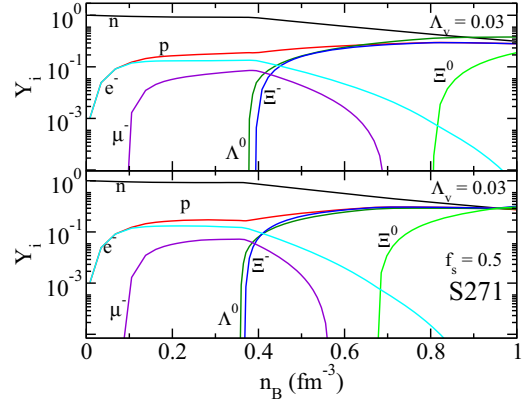


FIG. 4. The particle fractions Y_i of baryons and leptons as a function of baryon number density n_B in a neutron star with S271 (top panel) and S271 with $f_s = 0.5$ (bottom panel) for $\Lambda_v = 0.03$.

trend is similar in the appearance of hyperons for S271 with $f_s = 0.5$ for $\Lambda_v = 0.03$ in Fig. 4. As the objective of Fig. 4 is to elucidate the impact of the Λ_v coupling on the emergence of hyperons, our analysis indicates that hyperons manifest at slightly higher n_B values for $\Lambda_v = 0.03$ compared to $\Lambda_v = 0.00$. This feature is consistent because the EoS of hyperon-rich matter is slightly softer at high densities for $\Lambda_v = 0.03$. It should be noted that the Σ hyperon does not appear for both the values of Λ_v . The absence of the Σ hyperon in Figs. 3 and 4 could be attributed to the repulsive nature of the U_{Σ}^N interaction at nuclear saturation density.

We display our results of the mass-radius relationship using the S271 parameter set and S271 with $f_s = 0.5$ and 0.6 for $\Lambda_v = 0.00$ and 0.03 in the left and right panels of Fig. 5, respectively. For the crust region, we implemented the Baym-Pethick-Sutherland (BPS) EoS [44], and the crust-core transition is modeled as in Ref. [45]. The shaded region in both panels of Fig. 5 represents the observational constraints obtained from GW190814 [46], PSR J0740+6620 [10,11], PSR J0348+0432 [3], GW170817 [47], and the NICER experiment for PSR J0030+0451 [7,8], respectively. One can

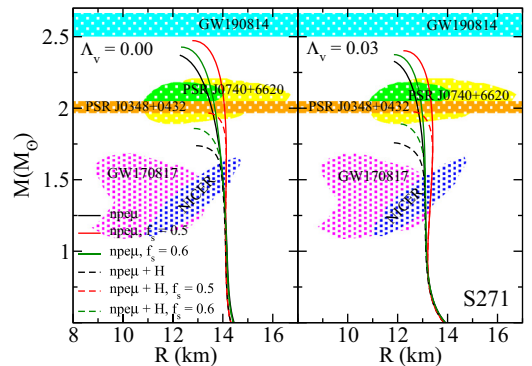


FIG. 5. The mass-radius relation of a neutron star with a σ -cut potential for pure nucleonic and hyperon-rich neutron star with S271 and S271 with $f_s = 0.5$ and 0.6 for $\Lambda_v = 0.00$ (left panel) and for $\Lambda_v = 0.03$ (right panel), respectively. The available astrophysical observational constraints are represented by the shaded region.

TABLE I. The maximum mass and radius of a neutron star are denoted by M_{\max} and R_{\max} , respectively. The global properties of a neutron star of mass $1.4M_{\odot}$, such as radius ($R_{1.4}$), compactness parameter ($C_{1.4}$), and tidal deformability ($\Lambda_{1.4}$) for $\Lambda_v = 0.00(0.03)$, are listed.

Parameter	M_{\max} (M_{\odot})	R_{\max} (km)	$R_{1.4}$ (km)	$C_{1.4}$	$\Lambda_{1.4}$
S271					
npe μ	2.37(2.33)	12.28(11.85)	14.05(13.10)	0.147(0.158)	946(576)
npe μ , $f_s = 0.5$	2.47(2.40)	12.78(12.23)	14.14(13.33)	0.146(0.155)	1014(673)
npe μ , $f_s = 0.6$	2.42(2.38)	12.32(11.85)	14.21(13.11)	0.147(0.158)	946(581)
npe μ + H	1.74(1.76)	12.93(11.85)	14.02(13.09)	0.148(0.158)	948(577)
npe μ + H, $f_s = 0.5$	1.97(1.97)	13.42(12.63)	14.15(13.33)	0.146(0.155)	1014(673)
npe μ + H, $f_s = 0.6$	1.86(1.89)	12.84(12.12)	14.04(13.11)	0.147(0.158)	946(581)

observe from Fig. 5 that all the EoS, irrespective of whether it is a pure nucleonic or hyperon rich, fit well within the limits of these constraints. As anticipated, neutron stars composed of only neutrons, protons, electrons, and muons, i.e., pure nucleonic matter exhibit a higher mass compared to hyperon-rich matter. For both neutron star compositions, i.e., pure nucleonic and hyperon-rich matter, the highest value of maximum mass corresponds to S271 with $f_s = 0.5$ for $\Lambda_v = 0.00$ as well as for $\Lambda_v = 0.03$, which can be seen from Fig. 5. We listed our results of neutron star properties for $\Lambda_v = 0.00$ and $\Lambda_v = 0.03$ in Table I. In Table I, the first and fourth rows display the results obtained for $\Lambda_v = 0.00$ belonging to the original S271 parameter set for pure nucleonic and hyperon-rich neutron stars, respectively.

From Table I, we found that the maximum mass (M_{\max}) of a pure nucleonic star is $2.37M_{\odot}$ for the S271 parameter set. Also, the radius ($R_{1.4}$) and tidal deformability ($\Lambda_{1.4}$) of a pure nucleonic star are 14.05 km and 946 for the S271 parameter set, respectively. Similarly, for hyperon-rich neutron star the M_{\max} , $R_{1.4}$, and $\Lambda_{1.4}$ are $1.74M_{\odot}$, 14.02 km and 948 for the S271 parameter set, respectively. So, from our present analysis, we can conclude that the inclusion of hyperons reduces the M_{\max} and has almost no effect on $R_{1.4}$ and $\Lambda_{1.4}$. We find the trend similar in the value of M_{\max} , $R_{1.4}$, and $\Lambda_{1.4}$ for pure nucleonic and hyperon-rich neutron stars even for S271 with $f_s = 0.5$ and 0.6. One can see that the highest value of the maximum mass of a pure nucleonic neutron star is $2.47M_{\odot}$ for $\Lambda_v = 0.00$ and $2.40M_{\odot}$ for $\Lambda_v = 0.03$, respectively. Similarly, the highest value of the maximum mass of hyperon-rich matter is $1.97M_{\odot}$ for both values of Λ_v . The trend is similar in the case of neutron star properties for both values of f_s as well. So, it is clear that the symmetry energy, i.e., Λ_v coupling has a negligible effect on the M_{\max} of neutron stars irrespective of the composition of neutron stars. However, for $f_s = 0.6$, there is a slight reduction in the mass of neutron stars for both compositions, compared to the masses for $f_s = 0.5$.

There is around a 4% increase in the maximum mass M_{\max} of a pure nucleonic neutron star for S271 with $f_s = 0.5$ compared to the S271 parameter set. Similarly, the maximum mass M_{\max} of a hyperon-rich neutron star increases by 13% for S271 with $f_s = 0.5$ compared to the S271 parameter set. This shows that $U_{\text{cut}}(\sigma)$ has an effect on the M_{\max} of a hyperon-rich neutron star compared to a pure nucleonic neutron star. On the other hand, if we compare the value of $R_{1.4}$ and $\Lambda_{1.4}$ for pure nucleonic as well as for hyperon-rich neutron star,

we find that there is less than a 1% increase in $R_{1.4}$ and less than a 7% increase for S271 with $f_s = 0.5$ compared to the S271 parameter set. So, comparatively $U_{\text{cut}}(\sigma)$ has more effect on M_{\max} than $R_{1.4}$ and $\Lambda_{1.4}$. The total variation in the $R_{1.4}$ and $\Lambda_{1.4}$, i.e., both pure nucleonic and hyperon-rich neutron star combined, we found that $R_{1.4}$ varies as $14.02 \leq R_{1.4} \leq 14.21$ km and $\Lambda_{1.4}$ varies as $946 \leq \Lambda_{1.4} \leq 1014$ for $\Lambda_v = 0.00$. Similarly, $R_{1.4}$ varies as $13.09 \leq R_{1.4} \leq 13.33$ km and $\Lambda_{1.4}$ as $576 \leq \Lambda_{1.4} \leq 673$ for $\Lambda_v = 0.03$. It is clearly evident that Λ_v has an effect on $R_{1.4}$ and it is more prominent on $\Lambda_{1.4}$. If we compare our results of $R_{1.4}$ for $\Lambda_v = 0.00$ and 0.03 with Neutron Star Interior Composition Explorer (NICER) x-ray telescopes provided simultaneously neutron star's mass and radius for PSR J0030+0451 with $R(1.44^{+0.15}_{-0.14}) = 13.02^{+1.24}_{-1.06}$ km [7] and $R(1.34^{+0.15}_{-0.14}) = 12.71^{+1.14}_{-1.19}$ km [8] and for J0740+6620 $R(2.08 \pm 0.07) = 13.7^{+2.6}_{-1.5}$ km [11] and $R(2.072^{+0.067}_{-0.066}) = 12.39^{+1.30}_{-0.98}$ km [10], we noticed that with the inclusion of Λ_v , $R_{1.4}$ decreases by about 7% for both pure nucleonic and hyperon-rich neutron star without $U_{\text{cut}}(\sigma)$. Similarly, for a finite value of $U_{\text{cut}}(\sigma)$ and Λ_v , $R_{1.4}$ also decreases by around 7% for both pure nucleonic and hyperon-rich neutron stars. The Λ_v has a more drastic effect on the value of $\Lambda_{1.4}$ for both pure nucleonic and hyperon-rich neutron stars with or without $U_{\text{cut}}(\sigma)$. There is around a 64% reduction in the value of $\Lambda_{1.4}$ for $\Lambda_v = 0.03$ compared to $\Lambda_v = 0.00$. The results with $\Lambda_v = 0.03$ for $\Lambda_{1.4}$ are more consistent with GW170817 observational data [50].

Additionally, the mass-radius relationship for neutron stars with $\Lambda_v = 0.03$ is more consistent with the observational constraints compared to $\Lambda_v = 0.00$. It is to be noted that the maximum mass obtained in our calculation, i.e., $2.47M_{\odot}$, is slightly less than the mass constraint from the GW190814 event. However, the mass constraint from the GW190814 event is not so stringent because the nature of the secondary compact component involved in GW190814 as a neutron star is not completely resolved [48,49]. We present our results of tidal deformability (Λ) for pure nucleonic as well as hyperon-rich neutron stars with S271 and S271 with $f_s = 0.5$ and 0.6 for $\Lambda_v = 0.00$ (left panel) and for $\Lambda_v = 0.03$ (right panel) in Fig. 6. The observational constraints from GW170817 are shown as shaded regions in both panels of Fig. 6. Our results of tidal deformability (Λ) are consistent with the observational constraints of GW170817. However, according to GW170817, the predicted value of $\Lambda_{1.4}$ is 190^{+390}_{-120} at a 90% confidence level [50]. We found that our result for tidal

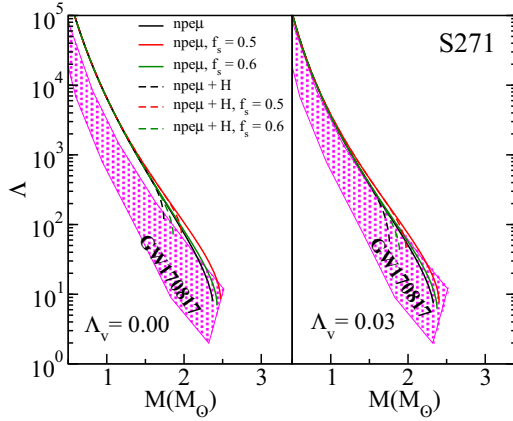


FIG. 6. The tidal deformability (Λ) of a neutron star as a function of mass M with S271 and S271 with $f_s = 0.5$ and 0.6 for pure nucleonic and nucleonic plus hyperon-rich neutron stars for $\Lambda_v = 0.00$ (left panel) and for $\Lambda_v = 0.03$ (right panel), respectively. The GW170817 observational data is represented by the shaded region.

deformability for pure nucleonic as well as hyperon-rich neutron stars for $\Lambda_v = 0.03$ is much closer to this predicted value of $\Lambda_{1.4}$ compared to $\Lambda_v = 0.00$. We also found that the compactness parameter ($C_{1.4}$) for a given Λ_v is almost the same for S271 and S271 with $f_s = 0.5$ and 0.6 irrespective of the composition of the neutron star.

In our previous work [21], we used the TM1* parameter set to construct the EoS to obtain the global properties of a neutron star. The TM1* is the extended version of TM1 with cross couplings, except for the Λ_v coupling. The main objective of that work was to investigate the effect of $U_{\text{cut}}(\sigma)$ on the composition and global properties of a neutron star. In comparison to our results of a pure nucleonic neutron star for the S271 parameter set with TM1* of Ref. [21], we found that the M_{max} and $\Lambda_{1.4}$ increase by around 17% and 12%, respectively, compared to TM1*. The main reason for this increase in M_{max} and $\Lambda_{1.4}$ is because S271 has no contribution from the nonlinear coupling of the ω meson, i.e., ζ_0 , which makes the EoS softer at high densities. Unlike M_{max} and $\Lambda_{1.4}$, the value of $R_{1.4}$ decreases by around 8.5% for S271 compared to TM1* [21]. Similarly, for a hyperon-rich neutron star, M_{max} and $\Lambda_{1.4}$ for S271 increase by around 9.5% and 12.6%, respectively, compared to TM1*. The $R_{1.4}$ for a hyperon-rich neutron star also decreases by around 8% for S271 compared to TM1*. While comparing the results of the present analysis with [21] for pure nucleonic as well as hyperon-rich neutron stars for S271 with $f_s = 0.6$, we found that for a given

parameter set, $U_{\text{cut}}(\sigma)$ has more or less the same effect on M_{max} , $R_{1.4}$, and $\Lambda_{1.4}$. Overall, our results of the present analysis are much closer to the observational data compared to previous work. It is also evident that neither $U_{\text{cut}}(\sigma)$ nor ζ_0 has any significant effect on $R_{1.4}$ and $\Lambda_{1.4}$, irrespective of whether it is a pure nucleonic or hyperon-rich neutron star. It is to be noted that TM1* has cross-coupling terms except Λ_v along with a finite value of ζ_0 . So, in the present work, we included the Λ_v term in our analysis with or without $U_{\text{cut}}(\sigma)$.

IV. CONCLUSIONS AND SUMMARY

The main objective of the present study is to analyze the effect of symmetry energy and the σ -cut potential on the composition and observational properties of neutron stars. Such studies are important to identify the parameters that can make the equation of state (EoS) consistent with the recent astronomical observational constraints. We considered pure nucleonic and hyperon-rich matter as neutron star compositions for the present study and implemented the σ -cut scheme along with the Λ_v coupling for the RMF model S271. As f_s is the free parameter in the σ -cut scheme, we chose S271 and S271 with $f_s = 0.5$ and 0.6 . We also took $\Lambda_v = 0.00$ and 0.03 to incorporate the symmetry energy effect in the present analysis.

In hyperon-rich neutron stars, we found that for a fixed value of Λ_v , hyperons occur at lower densities for S271 with $f_s = 0.5$ compared to S271, which indicates that f_s affects the densities at which the hyperons would start appearing. From our present analysis, we found that Λ_v has a more significant effect on tidal deformability compared to the mass and radius of a neutron star for a given value of f_s , and vice versa. We also found that there is not much difference in the properties of neutron stars for $f_s = 0.5$ and 0.6 , respectively. These effects of f_s and Λ_v do not change much with the composition, such as pure nucleonic and hyperon-rich neutron stars. However, we found that among all the EoS, the EoS of pure nucleonic neutron stars for S271 with $f_s = 0.5$ and $\Lambda_v = 0.03$ is the most consistent with astronomical constraints.

It is to be noted that in the present analysis, there is no contribution from the nonlinear term of the ω meson. Although our findings suggest that Λ_v has more effect on the global properties of neutron stars, a more detailed analysis is required, which includes other kinds of RMF EoS [51–53], before arriving at a conclusion. Such an analysis with non-nucleonic composition [54] other than hyperons and its comparison with astronomical constraints will be addressed in future works.

[1] M. Oertel, M. Hempel, T. Klöhn, and S. Typel, *Rev. Mod. Phys.* **89**, 015007 (2017).
 [2] J. M. Lattimer and M. Prakash, *Phys. Rep.* **621**, 127 (2016).
 [3] J. Antoniadis *et al.*, *Science* **340**, 6131 (2013).
 [4] P. Demorest, T. Pennucci, S. M. Ransom, M. S. E. Roberts, and J. W. T. Hessels, *Nature (London)* **467**, 1081 (2010).

[5] Z. Arzoumanian *et al.* (The NANOGrav Collaboration), *Astrophys. J. Suppl. Ser.* **235**, 37 (2018).
 [6] E. Fonseca *et al.*, *Astrophys. J. Lett.* **915**, L12 (2021).
 [7] M. C. Miller *et al.*, *Astrophys. J. Lett.* **887**, L24 (2019).
 [8] T. E. Riley *et al.*, *Astrophys. J. Lett.* **887**, L21 (2019).
 [9] P. Landry, R. Essick, and K. Chatziioannou, *Phys. Rev. D* **101**, 123007 (2020).

- [10] T. E. Riley *et al.*, *Astrophys. J. Lett.* **918**, L27 (2021).
- [11] M. C. Miller *et al.*, *Astrophys. J. Lett.* **918**, L28 (2021).
- [12] J.-L. Jiang, S.-P. Tang, Y.-Z. Wang, Y.-Z. Fan, and D.-M. Wei, *Astrophys. J.* **892**, 55 (2020).
- [13] S. Weissenborn, D. Chatterjee, and J. Schaffner-Bielich, *Phys. Rev. C* **85**, 065802 (2012).
- [14] M. Oertel, C. Providência, F. Gulminelli, and A. R. Raduta, *J. Phys. G* **42**, 075202 (2015).
- [15] Y. Yamamoto, T. Furumoto, N. Yasutake, and T. A. Rijken, *Phys. Rev. C* **88**, 022801(R) (2013).
- [16] Y. Yamamoto, T. Furumoto, N. Yasutake, and T. A. Rijken, *Phys. Rev. C* **90**, 045805 (2014).
- [17] K. A. Maslov, E. E. Kolomeitsev, and D. N. Voskresensky, *Phys. Rev. C* **92**, 052801(R) (2015).
- [18] Y. Zhang, J. Hu, and P. Liu, *Phys. Rev. C* **97**, 015805 (2018).
- [19] F. Ma, W. Guo, and C. Wu, *Phys. Rev. C* **105**, 015807 (2022).
- [20] M. Dutra, O. Lourenço, and D. P. Menezes, *Phys. Rev. C* **93**, 025806 (2016).
- [21] N. K. Patra, B. K. Sharma, A. Reghunath, A. K. H. Das, and T. K. Jha, *Phys. Rev. C* **106**, 055806 (2022).
- [22] C. Ducoin, J. Margueron, and C. Providência, *Europhys. Lett.* **91**, 32001 (2010).
- [23] M. Centelles, X. Roca-Maza, X. Viñas, and M. Warda, *Phys. Rev. Lett.* **102**, 122502 (2009).
- [24] F. J. Fattoyev, J. Piekarewicz, and C. J. Horowitz, *Phys. Rev. Lett.* **120**, 172702 (2018).
- [25] X. Roca-Maza, X. Viñas, M. Centelles, B. K. Agrawal, G. Coló, N. Paar, J. Piekarewicz, and D. Vretenar, *Phys. Rev. C* **92**, 064304 (2015).
- [26] J. M. Lattimer and A. W. Steiner, *Eur. Phys. J. A* **50**, 40 (2014).
- [27] I. Tews, J. M. Lattimer, A. Ohnishi, and E. E. Kolomeitsev, *Astrophys. J.* **848**, 105 (2017).
- [28] D. Adhikari *et al.* (PREX Collaboration), *Phys. Rev. Lett.* **126**, 172502 (2021).
- [29] B. T. Reed, F. J. Fattoyev, C. J. Horowitz, and J. Piekarewicz, *Phys. Rev. Lett.* **126**, 172503 (2021).
- [30] C. J. Horowitz and J. Piekarewicz, *Phys. Rev. Lett.* **86**, 5647 (2001).
- [31] A. Gal, *Prog. Theor. Phys. Suppl.* **186**, 270 (2010), and reference therein.
- [32] J. R. Oppenheimer and G. M. Volkoff, *Phys. Rev.* **55**, 374 (1939).
- [33] R. C. Tolman, *Phys. Rev.* **55**, 364 (1939).
- [34] J. M. Lattimer and M. Prakash, *Science* **304**, 536 (2004).
- [35] P. G. Krastev and F. Sammarruca, *Phys. Rev. C* **74**, 025808 (2006).
- [36] È. È. Flanagan and T. Hinderer, *Phys. Rev. D* **77**, 021502(R) (2008).
- [37] T. Hinderer, *Astrophys. J.* **677**, 1216 (2008).
- [38] T. Hinderer, B. D. Lackey, R. N. Lang, and J. S. Read, *Phys. Rev. D* **81**, 123016 (2010).
- [39] T. Damour, A. Nagar, and L. Villain, *Phys. Rev. D* **85**, 123007 (2012).
- [40] S. Postnikov, M. Prakash, and J. M. Lattimer, *Phys. Rev. D* **82**, 024016 (2010).
- [41] G. A. Lalazissis, J. König, and P. Ring, *Phys. Rev. C* **55**, 540 (1997).
- [42] J. Xu, A. Carbone, Z. Zhang, and C. M. Ko, *Phys. Rev. C* **100**, 024618 (2019).
- [43] C. Drischler, R. J. Furnstahl, J. A. Melendez, and D. R. Phillips, *Phys. Rev. Lett.* **125**, 202702 (2020).
- [44] G. Baym, C. Pethick, and P. Sutherland, *Astrophys. J.* **170**, 299 (1971).
- [45] T. Malik, K. Banerjee, T. K. Jha, and B. K. Agrawal, *Phys. Rev. C* **96**, 035803 (2017).
- [46] R. Abbott *et al.*, *Astrophys. J. Lett.* **896**, L44 (2020).
- [47] B. P. Abbott *et al.* (LIGO Scientific Collaboration and Virgo Collaboration), *Phys. Rev. X* **9**, 011001 (2019).
- [48] A. Sedrakian, F. Weber, and J. J. Li, *Phys. Rev. D* **102**, 041301(R) (2020).
- [49] J. J. Li, A. Sedrakian, and F. Weber, *Phys. Lett. B* **810**, 135812 (2020).
- [50] B. P. Abbott *et al.* (The LIGO Scientific Collaboration and the Virgo Collaboration), *Phys. Rev. Lett.* **121**, 161101 (2018).
- [51] J. K. Bunta and S. Gmuca, *Phys. Rev. C* **68**, 054318 (2003).
- [52] B. G. Todd-Rutel and J. Piekarewicz, *Phys. Rev. Lett.* **95**, 122501 (2005).
- [53] S. Typel and H. H. Wolter, *Nucl. Phys. A* **656**, 331 (1999).
- [54] P. Ribes, A. Ramos, L. Tolos, C. Gonzalez-Boquera, and M. Centelles, *Astrophys. J.* **883**, 168 (2019).